Ecotoxicology and Environmental Safety 273 (2024) 116090

Contents lists available at ScienceDirect

Ecotoxicology and Environmental Safety

journal homepage: www.elsevier.com/locate/ecoenv

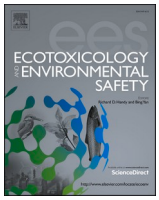

Diesel exhaust particle exposure exacerbates ciliary and epithelial barrier dysfunction in the multiciliated bronchial epithelium models

Eunsook Park [a], Bu-Yeo Kim [b], Seahyoung Lee [c], Kuk Hui Son [d], Jihye Bang [a], Se Hyang Hong [a], Joong Won Lee [a], Kyung-Ok Uhm [a], Hyun-Jeong Kwak [e], Hyun Joung Lim [a,*]

[a] Division of Allergy and Respiratory Disease Research, Department of Chronic Disease Convergence Research, Korea National Institute of Health, Korea Disease Control and Prevention Agency, Chungju, Chungcheongbuk-do 28159, South Korea
[b] Herbal Medicine Research Division, Korea Institute of Oriental Medicine, Daejeon 34054, South Korea
[c] Institute for Bio-Medical Convergence, College of Medicine, Catholic Kwandong University, Gangneung-si, Gangwon-do, South Korea
[d] Department of Thoracic and Cardiovascular Surgery, Gachon University Gil Medical Center, College of Medicine, Gachon University, Incheon 215565, South Korea
[e] Department of Bio and Fermentation Convergence Technology, Kookmin Univerisity, Seonbuk-Gu, Seoul 02707, South Korea

ARTICLE INFO

Edited by: Bing Yan

Keywords:
Diesel exhaust particle
Normal human bronchial epithelial cell
Air-liquid interface
Ciliary function
Mucociliary clearance

ABSTRACT

Airway epithelium, the first defense barrier of the respiratory system, facilitates mucociliary clearance against inflammatory stimuli, such as pathogens and particulates inhaled into the airway and lung. Inhaled particulate matter 2.5 ($PM_{2.5}$) can penetrate the alveolar region of the lung, and it can develop and exacerbate respiratory diseases. Although the pathophysiological effects of $PM_{2.5}$ in the respiratory system are well known, its impact on mucociliary clearance of airway epithelium has yet to be clearly defined. In this study, we used two different 3D in vitro airway models, namely the EpiAirway-full-thickness (FT) model and a normal human bronchial epithelial cell (NHBE)-based air-liquid interface (ALI) system, to investigate the effect of diesel exhaust particles (DEPs) belonging to $PM_{2.5}$ on mucociliary clearance. RNA-sequencing (RNA-Seq) analyses of EpiAirway-FT exposed to DEPs indicated that DEP-induced differentially expressed genes (DEGs) are related to ciliary and microtubule function and inflammatory-related pathways. The exposure to DEPs significantly decreased the number of ciliated cells and shortened ciliary length. It reduced the expression of cilium-related genes such as acetylated α-tubulin, ARL13B, DNAH5, and DNAL1 in the NHBEs cultured in the ALI system. Furthermore, DEPs significantly increased the expression of MUC5AC, whereas they decreased the expression of epithelial junction proteins, namely, ZO1, Occludin, and E-cadherin. Impairment of mucociliary clearance by DEPs significantly improved the release of epithelial-derived inflammatory and fibrotic mediators such as IL-1β, IL-6, IL-8, GM-CSF, MMP-1, VEGF, and S100A9. Taken together, it can be speculated that DEPs can cause ciliary dysfunction, hyperplasia of goblet cells, and the disruption of the epithelial barrier, resulting in the hyperproduction of lung injury mediators. Our data strongly suggest that PM2.5 exposure is directly associated with ciliary and epithelial barrier dysfunction and may exacerbate lung injury.

1. Introduction

Airway epithelium, located in the trachea and brioche of the respiratory system, is the first defense barrier against inhaled pathogens, allergens, and particulates (Adivitiya et al., 2021; Knowles and Boucher, 2002). In healthy airway epithelium, inhaled pathogens and particles are removed, being trapped in the mucus secreted by goblet cells in the form of sputum by ciliary motility of ciliated cell particulates (Adivitiya et al., 2021; Knowles and Boucher, 2002). Ciliary dysfunction, such as abnormal motility, length, and structure, is associated with abnormal mucociliary clearance, such as hypersecretion of mucus, weakening of tight junction, and inflammatory response in the epithelium

Abbreviations: $PM_{2.5}$, Particulate matter 2.5; NHBE, normal human bronchial epithelial cell; ALI, air-liquid interface; DEP, diesel exhaust particle; DEG, differentially expressed gene; COPD, chronic obstructive pulmonary disease; CF, cystic fibrosis; PCD, primary ciliary dyskinesia; SRM, standard reference material; GO, gene ontology; IL, interleukin; TEER, transepithelial electrical resistance; ZOs, zona occludins.

* Correspondence to: Division of Allergy and Respiratory Disease Research, Department of Chronic Disease Convergence Research, Korea National Institute of Health, Korea Disease Control and Prevention Agency, Chungju 28159, South Korea.
E-mail address: hjlim1121@korea.kr (H.J. Lim).

https://doi.org/10.1016/j.ecoenv.2024.116090
Received 25 September 2023; Received in revised form 30 January 2024; Accepted 6 February 2024
Available online 15 February 2024

(Bustamante-Marin and Ostrowski, 2017; Carlier et al., 2021).

Particulate matter (PM), a major component of air pollutants, is classified as coarse particles (PM_{10}, particles $\leq$ 10 μm in diameter), fine particles ($PM_{2.5}$, particles $\leq$ 2.5 μm in diameter), and ultrafine particles ($PM_{0.1}$, particles $\leq$ 0.1 μm in diameter. In respiratory systems, PM_{10} and $PM_{2.5}$ can penetrate the primary bronchial tract and alveolar region, respectively, whereas $PM_{0.1}$ can cross cell membranes and directly affect cells (Yang et al., 2020). Inhalation of PM is associated with developing and exacerbating respiratory diseases such as asthma, COPD (chronic obstructive pulmonary disease), and lung cancer. Previous studies have demonstrated that the underlying mechanisms of PMs to cause respiratory diseases include innate immune inflammation, oxidative stress, apoptosis, autophagy, and imbalance of Th1/Th2 cells (Leikauf et al., 2020; Mazzarella et al., 2007).

Recent studies have shown that exposure to $PM_{2.5}$ can induce cilia shortening, mucus production, and a collapse of the tight junction with oxidative stress in bronchial epithelial cells (Kim et al., 2017, 2021). However, these results were obtained from submerged cultures of bronchial epithelial cells, which does not allow one to assess cilia function. Therefore, they may not be appropriate to accurately address the process of $PM_{2.5}$-induced ciliary dysfunction and impairment of mucociliary clearance. On the contrary, the bronchial epithelial cell model used in the present study involves bronchial epithelial cells differentiated at the air-liquid interface (ALI), and thus is physiologically more relevant as it is comparable to the airway epithelium model, representing an environment of pseudostratified epithelium that comprises motile cilia, mucus secretion, and epithelial barrier (Gray et al., 1996; Stewart et al., 2012). $PM_{2.5}$ exposure exacerbates the disruption of the epithelial barrier composed of epithelial cells grown in ALI with upregulated production of pro-inflammatory cytokines, such as IL-6 and IL-8, and reactive oxygen species (ROS). This suggests that the underlying mechanism of the $PM_{2.5}$-induced disruption of the airway epithelium defense system involves the production of oxidative stress and inflammatory responses (Ghio et al., 2013; He et al., 2020; Zarcone et al., 2016). Moreover, diesel exhaust particles (DEPs), a mixture of organic chemicals and metals, are the main component of $PM_{2.5}$ and are reportedly associated with airway inflammation and remodeling through cytotoxicity, DNA damage, and oxidative stress (Li et al., 2006; Steiner et al., 2016). Nevertheless, unlike other harmful factors such as cigarette smoke and viral infections, detailed mechanisms of how $PM_{2.5}$, including DEPs, exposure causes cilia dysfunction and impaired mucociliary clearance of the airway defense machinery have not been elucidated.

In this study, we investigated the effect of DEPs on the airway defense machinery's ciliary function and mucociliary clearance. EpiAirwayFT tissues simulating 3D full-thickness (FT) respiratory human microtissues were subjected to a transcriptomic analysis, and the transcriptomic changes were further confirmed by using ALI-cultured primary normal human bronchial epithelial cells (NHBEs). DEPs in the multiciliated epithelium model lead to ciliary dysfunction, hyperplasia of goblet cells, disruption of the epithelial barrier, and hyperproduction of lung injury mediators. These results provided insights for understanding the molecular and cellular bases for impaired airway defense machinery by DEP exposure in the multiciliated epithelium model.

2. Materials and methods

2.1. Preparation and exposure of DEPs

DEPs, diesel PM standard reference material (SRM) 1650b, were commercially obtained from the National Institute of Standards and Technology (NIST, Gaithersburg, MD). DEPs (20 mg/mL) were suspended in 10% dimethyl sulfoxide (DMSO) (Sigma-Aldrich, Burlington, MA) with Dulbecco's phosphate-buffered saline (DPBS) and sonicated for 1 h with vortexing in a cooling water bath. Dissolved DEPs were aliquoted and stored for a short period at −20 ℃ and a long period at −70 ℃ for further analysis. Before cell exposure, thawed DEPs were sonicated for 1 h in a cooling water bath and freshly resuspended in DPBS. DEP suspension (100 μL) with DPBS was treated directly to the apical side of the transmembrane and exposed to EpiAirwayFT tissue (AFT-100, MatTek, Ashland, MA) or ALI-cultured NHBEs. DMSO (10%) with dPBS was used as a vehicle.

2.2. RNA-sequencing analysis

The libraries were prepared for 150 bp paired-end sequencing using TruSeq Stranded mRNA Library Prep Kit (Illumina, San Diego, CA, USA). Total RNA from the EpiAirwayFT tissues exposed to DEPs for 24 or 72 h was extracted using Trizol reagent (Thermo Fisher Scientific, Waltham, MA, USA), and a total of 500 ng of RNA molecules were fragmented and synthesized as single-stranded cDNAs through random hexamer priming. The products were used as a template for second-strand synthesis, and double-stranded cDNA was prepared. After sequential processes of end repair, A-tailing, and adapter ligation, the cDNA libraries were amplified. The libraries were quality-checked using the TapeStation 4200 instrument and High Sensitivity D1000 ScreenTape System (Agilent, Santa Clara, CA, USA). According to the manufacturer's library quantification protocol, they were quantified with the KAPA library quantification kit (Kapa Biosystems, Wilmington, MA, USA). Following cluster amplification of denatured templates, sequencing was performed as paired-end (2×150 bp) using Illumina Novaseq6000 (Illumina). Finally, the normalized gene count was measured as fragments per kilobase of transcript per million mapped reads (FPKM).

To measure gene expression profiling, genes exhibiting an expression change of at least 1.5-fold increase (or decrease) compared to control were selected from samples and hierarchically clustered according to expression similarity using the Gene Cluster 3.0 program (De Hoon et al., 2004). Volcano plots for gene expression were generated using the EnhancedVolcano package (version 1.16.0) in R. To measure the network structure of Gene Ontologies (GOs) related to gene function, a list of genes with more than 1.5-fold increase (or decrease) compared to the control group was selected and analyzed with the ClueGO program at default parameter settings (Bindea et al., 2009). To determine gene-related GO terms, the clusterProfiler 4.0 package in R was used (Wu et al., 2021). As previously reported (Kim et al., 2018, 2020, 2022), pathway activity was calculated by summing the gene expression rates in each pathway obtained from the KEGG pathway database (https://www.genome.jp/kegg/). Only pathways in which 50% or more of the genes constituting the pathway were present were analyzed. Specifically, the expression ratios of the genes compared to that of the control were logarithmically transformed and linearly added. In this process, genes (or proteins) that inhibit the main flow of signals in the pathway were given a weight of −1. To determine the statistical significance of pathway activity, the measured pathway activity was compared with random activity values obtained by repeating the same process 1000 times with randomly selected genes.

2.3. ALI-cultured NHBEs

NHBEs (Lonza, Walkersville, MD, USA) were cultured in 0.1 mg/mL collagen IV-coated tissue culture dish with PneumaCult-Ex Plus medium (STEMCELL Technologies, Vancouver, Canada) supplemented with 1% penicillin-streptomycin and incubated at 37 °C with 5% CO_2. For ALI culture, NHBEs (1.5×10^5 cells/well) were seeded onto collagen IV-coated polyester (PET) membrane 12 mm Transwell (3460, Corning, NY, USA) and incubated in PneumaCult-Ex Plus medium added to both the apical and basolateral sides of Transwell inserts until the cells reached 100% confluency (Rayner et al., 2019). Then, the medium on the apical side of the Transwell inserts was removed. At the same time, the medium on the basolateral side was changed to PneumaCult-ALI medium (STEMCELL Technologies) containing supplements. Cells at ALI were cultured for 20 d and washed with DPBS on the apical side, and

the medium was changed on the basolateral side every 2–3 d.

2.4. Immunofluorescence staining

For immunofluorescence staining of the Transwell membrane, the inserts were washed with PBS and fixed with 4% paraformaldehyde (PFA; Biosesang, Seongnam, Korea) for 20 min. Cells were permeabilized with 0.1% Triton X-100 in PBS for 10 min and blocked with 1% bovine serum albumin (BSA) in PBS+0.1% Tween 20 (PBST) for 30 min. Primary antibodies including ARL13B (17711–1-AP; Proteintech, Rosemont, IL, USA), acetylated α-tubulin (sc-23950; Santa Cruz Biotechnology, Santa Cruz, CA, USA), E-cadherin (#3195; Cell signaling, Denver, MA, USA), phalloidin (A12381; Invitrogen, Carlsbad, CA, USA) and MUC5AC (orb547405; Biorbyt, Cambridge, UK) were diluted with 1% BSA in PBST and incubated with cells for 1 h at room temperature. Fluorescence-conjugated secondary antibodies, including Alexa Fluor 488 goat anti-rabbit IgG and Alexa Fluor 594 goat anti-mouse IgG (Invitrogen), were incubated with cells for 1 h in the dark at room temperature. The Transwell membranes were cut and mounted on glass slides. Membranes on the slide were covered with the coverslip, and fluorescence images were visualized by an FV3000-ORS laser scanning confocal microscope (Olympus Crop., Tokyo, Japan). To access areas of the fluorescence-positive cells, fluorescent intensity was measured using cellSens imaging software (ver 2. X) (Olympus).

For immunofluorescence staining of single-ciliated cells, they were dissociated from the Transwell inserts using TrypLE Express (Gibco, Grand Island, NY, USA) and fixed with 4% PFA for 10 min. After washing with PBS, the cells were resuspended in it in a total volume of 400 μL. Aliquots of 100 μL of cell suspension were centrifuged on a glass slide at 500 rpm for 5 min using a cytospin centrifuge (Hanil Science Industrial, Seoul, Korea), and immunofluorescence staining was performed with acetylated α-tubulin antibody, as mentioned above. Cells on the slide were covered with the coverslip with ProLong Gold antifade reagent with 4′,6-diamidino-2-phenylindole (DAPI) (Invitrogen). To measure cilia length, 230 cilia in each group were analyzed (10 cilia on each of 23 ciliated cells) using the ImageJ open source.

2.5. Hematoxylin and Eosin (H&E) staining and Alcian blue (AB) staining

The Transwell was fixed overnight in 4% PFA, dehydrated, and paraffin embedded. After deparaffinization and rehydration, paraffin sections were stained with either hematoxylin, eosin (H&E), or AB and then covered with a cover slip with an aqueous mounting medium. Sections stained with AB 8GX (Sigma-Aldrich) were counterstained with nuclear fast red (Sigma-Aldrich). Images were acquired with the Pannoramic SCAN II slide scanner (3D Histech, Budapest, Hungary).

2.6. Transmission electron microscopy (TEM)

To determine an ultrastructure of the differentiated cilium, the cells were pre-fixed with a fresh solution containing 2.5% glutaraldehyde and 2% formaldehyde at 4 °C and then post-fixed with 1% osmium tetroxide. The specimens were dehydrated, embedded in Epon 812, and sectioned in 70 nm thick slices. Double staining was performed with 5% aqueous uranyl acetate for 10 min and 3% lead citrate for 60 s. The sections were examined using TEM LIBRA120 (ZEISS, Oberkochen, Germany).

2.7. Western blot analysis

Cells were lysed in PRO-PREP Protein Extraction Solution (iNtRON, Seoul, Korea) by vortexing. The protein lysates (10 μg) were separated on Bolt 4–12% Bis-Tris Plus mini gels (Invitrogen) and transferred to a polyvinylidene difluoride membrane using Trans-Blot Turbo Transfer System (Bio-Rad Laboratories, Hercules, CA, USA). Membranes were blocked in 5% skim milk with PBST for 1 h at room temperature and incubated with primary antibodies against ARL13B (Proteintech), acetylated α-tubulin (Santa Cruz Biotechnology), E-cadherin (Cell signaling), ZO1 (ab96587; Abcam, Cambridge, UK) and β-actin (sc-47778; Santa Cruz Biotechnology) overnight at 4 °C. After washing with PBST; the membrane was incubated with horseradish peroxidase-conjugated secondary antibodies and developed using the Super-Signal West Femto Maximum Sensitivity Substrate (Thermo Fisher Scientific). Signals were detected using a ChemiDoc Imaging System (Bio-Rad Laboratories), and band intensity was quantified using Image Lab software (Bio-Rad Laboratories).

2.8. Quantitative real-time PCR (qRT-PCR)

Total RNA was prepared from cut membranes of the Transwell inserts using RNAeasy Mini Kit (Qiagen, Germantown, MD, USA) according to the manufacturer's instructions. cDNA from 1 μg of total RNA was synthesized using RNA to cDNA EcoDry Premix (TaKaRa, Shiga, Japan). qRT-PCR was performed using the PowerSYBR Green PCR Master Mix (Applied Biosystems, Warrington, UK) on QuantStudio5 real-time PCR system (Applied Biosystems) according to the manufacturer's instructions. The gene primer sequences used are as follows: DNAH5-F: 5′-CGTGGAGTGCATCATCAGTG-3′, DNAH5-R: 5′-TCTTGGTTTGCACGGGAATG-3′, DNALI1-F: 5′-CACCTCCAGGAGCAGTTAGAC-3′, DNALI1-R: 5′-TGACCTCCCGGATCAACTCA-3′, β-actin-F: 5′-CCAACCGCGAGAAGATGA-3′, β-actin-R: 5′-CCAGAGGCGTACAGGGATAG-3′ (Schamberger et al., 2015).

2.9. Transepithelial electrical resistance (TEER) measurement

Before the measurement of TEER, the apical surfaces of the Transwell were rinsed with PBS. At pre- and 72 h post-exposure of DEPs, TEER was measured with an electrometer EVOM2 (World Precision Instruments, Sarasota, FL) using an STX electrode. The TEER values were calculated as unit area resistance (Ohm × cm^2) and presented as percent relative to the pre-exposure values.

2.10. Enzyme-linked immunosorbent assay (ELISA) and Luminex assay

After DEP exposure on the apical side of the Transwell inserts, the basolateral medium was harvested and stored at −70 ℃. Levels of secretory factors, interleukin (IL)−1β, IL-6, granulocyte-macrophage colony-stimulating factor (GM-CSF), matrix metalloproteinase-1 (MMP-1), S100 calcium-binding protein A9 (S100A9), and vascular endothelial growth factor (VEGF) were quantified from basolateral medium using Luminex assay according to the manufacturer's instructions (R&D Systems, Minneapolis, MN, USA). IL-8 (R&D systems), MUC5AC (Biomatik, Ontario, Canada), and MUC5B (Biomatik) levels were measured using an ELISA kit according to the manufacturer's instructions.

2.11. Statistical analysis

All data in HNBEs are presented as the standard error of the mean (SEM) in at least three independent experiments. Statistical significance was calculated by two-tailed unpaired Student's t-test using the GraphPad Prism5 software (GraphPad Software, Inc., San Diego, CA, USA). Statistical significance was set at $P \leq 0.05$ for all analyses.

3. Results

3.1. Expressional profile of genes, pathway activity, and functional enrichment

To investigate how DEPs affect the airway defense machinery, the change of the gene expressions in EpiAirwayFT apically exposed to DEPs for 24 or 72 h was accessed using RNA-sequencing analysis. As shown in Fig. 1, long-term exposure (72 h) to DEPs induced more dramatic gene

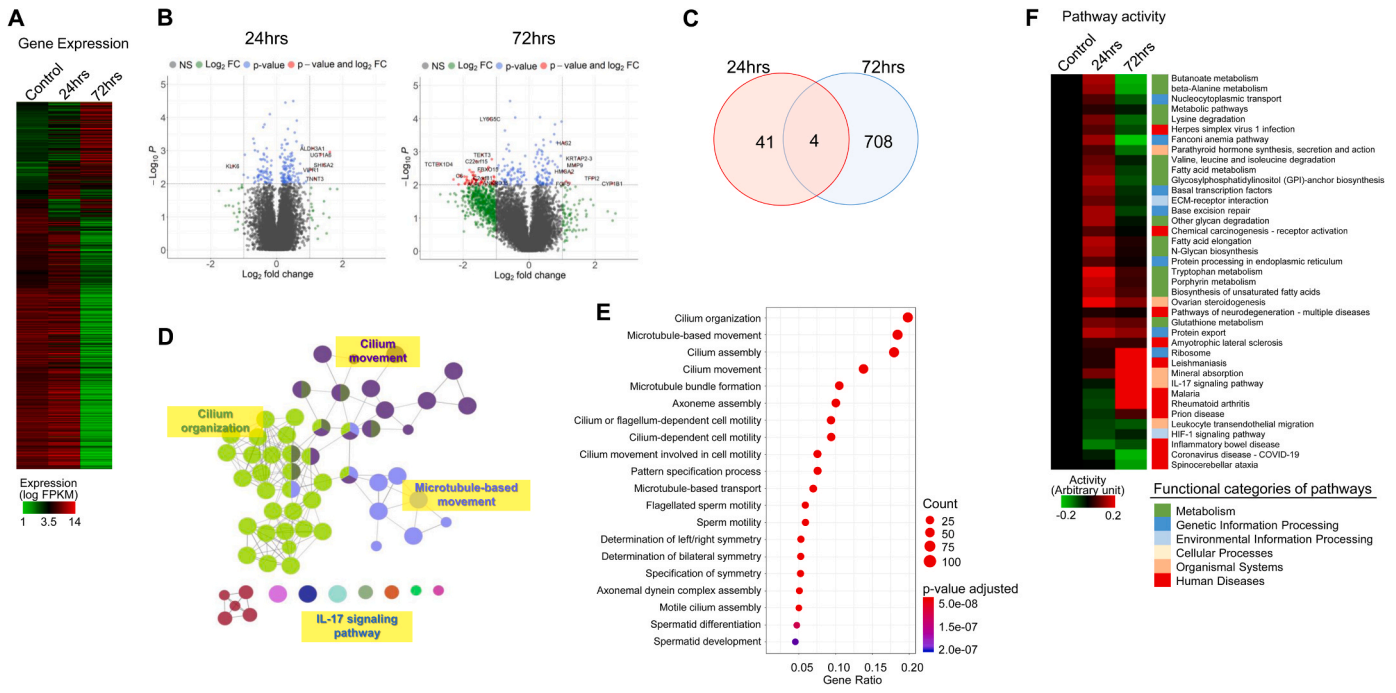

Fig. 1. Effects of DEP exposure on gene expression in an EpiAirwayFT. (A) A total of 2120 genes showing at least a 1.5-fold change in expression by exposure to DEPs at 24 or 72 h were clustered according to their expression level. Each row represents a gene in red or green, respectively, according to its high and low expression levels (logarithmic FPKM), as indicated by the scale bar. (B) Expression patterns of genes compared to that of the control are shown in a Volcano plot. The log fold represents the average expression level of each gene, and the log P-value represents the p-value of the Student's t-test for each gene. (C) After isolating DEGs with at least a 2-fold change compared to that of the control in each sample, their distributions were compared. (D) Enriched GO terms (FDR < 0.01) are shown as a network graph where each node represents a GO term, and node size is proportional to the number of genes associated with a GO term. Closely related GO terms are shown in the same color. Representative GO terms are indicated. (E) The top 20 GO terms selected from DEGs at 72 h are plotted. (F) Pathways showing a p-value <0.01 were selected from samples and clustered according to activity level relative to control. As the scale bar indicates, red and green colors represent high and low activity levels, respectively, compared to the control. According to KEGG's criteria, pathways were classified into six functional categories as indicated by color bars.

expression changes than 24 h exposure compared to that in the control (Fig. 1A and B). The distribution of the DEGs (increased more than 2-fold or decreased less than 0.5-fold compared to that of the control) upon DEP exposure significantly differed between the two time points (Fig. 1C). GO and KEGG pathway analysis indicated that the DEGs at 72 h were significantly enriched in ciliary and microtubule function ($p<0.001$) (Fig. 1D and E). We evaluated the pathway activity altered by DEP exposure using all genes involved in each pathway for a more general measure of biological function. Fig. 1F shows that inflammatory-related pathways were upregulated, whereas metabolic-related pathways were downregulated following 72 h exposure to DEPs compared to those in the control. These data suggest that the effect of DEPs against airway defense machinery may be associated with the regulation of ciliary function.

3.2. *Establishment of fully differentiated NHBECs as ALI cultures*

To further verify whether the observed DEP-induced transcriptomic changes indeed led to actual ciliary dysfunction, a multiciliated epithelium model using NHBEs was established. NHBEs were cultured in ALI condition for 20 d (Supplementary Fig. 1), and their differentiation was assessed on days 0, 14, 17, and 20 in ALI using immunofluorescent staining. The expression of acetylated α-tubulin, a marker of motile cilia, was only detected in the mitotic spindle of proliferating cells at day 0. Still, as the ALI-cultured cells form cilia, it was detected in the cilia-differentiated NHBEs (Day 14). Furthermore, the number of acetylated α-tubulin-positive cells gradually increased with time thereafter up to day 20 of ALI culture. The expression of acetylated α-tubulin was also correlated with the expression of ciliary protein ARL13B (Supplementary Fig. 1 A). Moreover, the ultrastructure of the '9+2' arrangement of microtubules was present in the cilia of differentiated NHBEs at ALI-cultured samples, indicating that ALI culture of NHBEs properly facilitated motile cilia formation (Supplementary Fig. 1B). Furthermore, ALI-cultured NHBEs expressed E-cadherin and F-actin, markers of tight junction, indicating that ALI-cultured NHBEs developed major components of the epithelial barrier (Supplementary Fig. 1 C). These data suggest that the differentiation of NHBEs in ALI culture adequately supported the structural organization of airway defense machinery required for mucociliary clearance and tight junction.

3.3. *DEP exposure affects ciliated to goblet cell ratio in fully differentiated NHBE cells*

To examine the effect of DEPs on a multiciliated epithelium, ALI-cultured NHBEs were exposed apically to DEPs for 72 h (Fig. 2A), and morphological changes were evaluated by H&E staining and AB staining. The results indicated that the DEP treatment decreased the number of cilia, whereas increasing the mucus secretion of the apical surface of the epithelium. However, the thickness of epithelium was not significantly changed by DEP treatment (Fig. 2B). Additional immunofluorescence staining using antibodies against acetylated α-tubulin and MUC5AC also indicated that DEPs decreased the area of ciliated cells (acetylated α-tubulin-positive cells), but increased the area of mucus-producing goblet cells (MUC5AC-positive cells) (Fig. 2C–F). These data suggest that DEPs may impair mucociliary clearance in ALI-cultured NHBEs.

3.4. *DEP exposure alters ciliary function-related gene expression in ALI-cultured NHBEs*

To evaluate the possibility of DEP-induced impairment of mucociliary clearance, the effect of DEP on the length of cilia and the expression

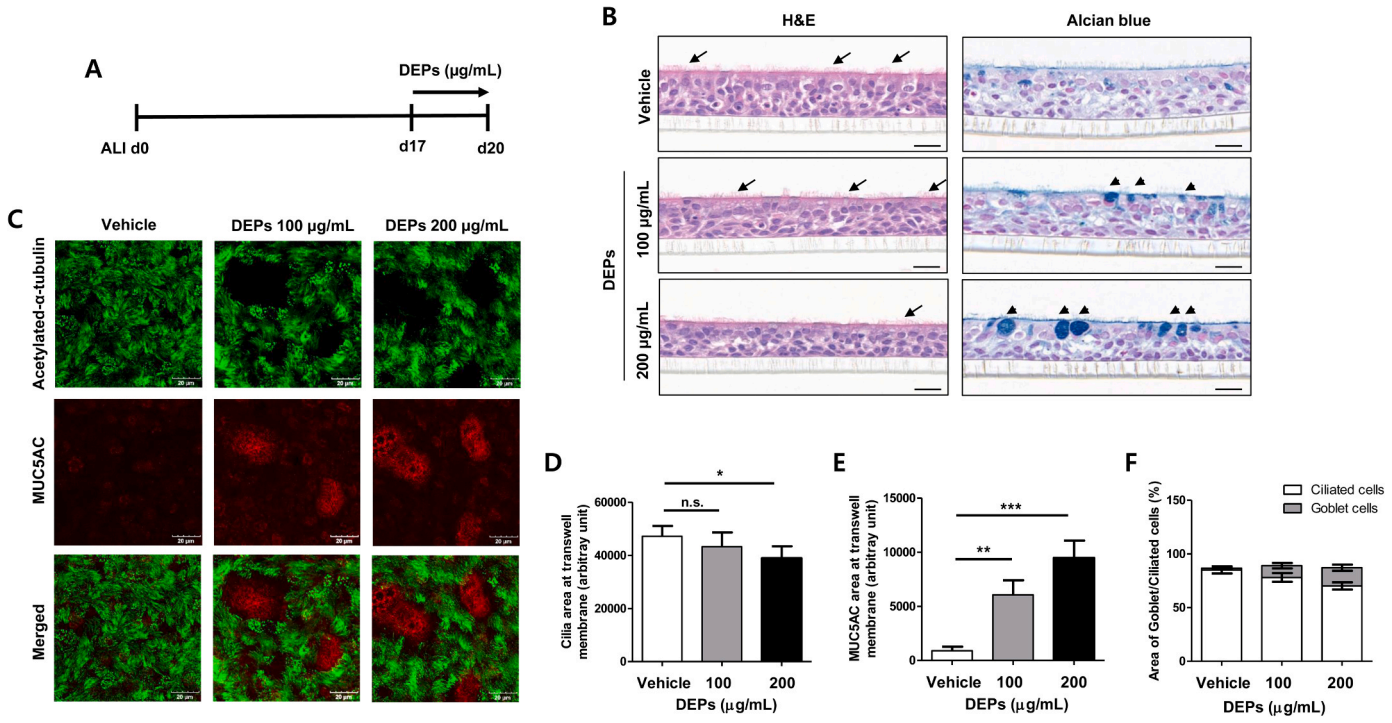

Fig. 2. DEPs change the ratio of ciliated and goblet cells in ALI-cultured NHBEs. (A) Experimental design of DEP treatment for 72 h on an apical side of the Transwell inserts. (B) Paraffin section of an ALI-cultured NHBEs exposed to DEPs was stained with H&E (*left*) and Alcian blue (*right*). Arrows and arrowheads indicate ciliated cells and goblet cells, respectively. (C) Representative immunofluorescence images of acetylated α-tubulin (green) and MUC5AC (red) after DEP treatment for 72 h. Bar: 20 μm. (D-F) Quantitative assessment of cilia and goblet cells-positive area in DEP-treated ALI-cultured NHBEs (n=3). Acetylated α-tubulin (D) and MUC5AC (E) positive area of Transwell membrane were measured with image J software and calculated as the percentage of MUC5AC / cilia area (F). n.s. > 0.05, *$P < 0.05$, **$P < 0.01$ and ***$P < 0.001$, compared with vehicle.

of motile cilia-related genes was examined. Compared to the vehicle-exposed cells, the DEP-exposed cells had significantly shorter cilia, and the length of the cilia was inversely proportional to the concentration of DEP used (Fig. 3A). DEP exposure also significantly suppressed the mRNA levels of DNAH5 and DNALI1, major components of cilia dynein, as well as protein levels of acetylated α-tubulin, ARL13B and ciliary protein markers DNAL1 and FOXJ1 (Fig. 3B and C). These results suggest that DEP may promote mucociliary clearance impairment by hindering sufficient production of motile cilia.

3.5. DEP exposure disrupts the epithelial barrier in ALI-cultured NHBEs

Impairment of mucociliary clearance in the airway epithelium leads to dysfunction of the airway barrier, which triggers the secretion of inflammation-related cytokines from epithelial cells. The expression of intracellular junction-related protein was examined to address the impact of DEPs on the airway epithelium barrier function. Immunofluorescence staining of acetylated-α-tubulin indicated that DEP caused loss of ciliated cells in a concentration-dependent manner. It also disrupted the formation of the normal epithelial layer (Fig. 4A). Western blot analysis showed that DEP treatment significantly suppressed the expression of tight junction proteins ZO-1 and Occludin and adherent protein E-cadherin (Fig. 4B). The results of TEER measurement indicated that the integrity of cellular barrier was significantly compromised by 200 μg/mL of DEP treatment. In contrast, a lower concentration of DEP (100 μg/mL) did not significantly affect the TEER (Fig. 4C). These data suggested that DEP can cause dysfunction of the airway barrier by compromising the epithelial layer integrity.

3.6. DEPs stimulate the secretion of inflammation and/or fibrosis-related regulators in ALI cultures

The amount of such mediators contained in the basolateral medium was examined to test the possibility of DEP contributing to the impairment of mucociliary clearance by producing inflammatory and fibrotic mediators. Apical exposure to DEPs increased the production of pro-inflammatory cytokines such as IL-1β, IL-6, IL-8, and GM-CSF in ALI-cultured NHBEs (Fig. 5A–D). Additionally, inflammatory and/or fibrotic mediators such as MMP-1, VEGF, and S100A9 significantly increased in response to DEP exposure (Fig. 5E–G).

4. Discussion

Typically, the cilium has a 9+2 array of microtubules with nine outer doublet microtubules and a central pair of singlet microtubules (Loreng and Smith, 2017). However, abnormal structures of cilia, such as dynein arm defects associated with reduced frequency of ciliary beating, are predominantly observed in patients with primary ciliary dyskinesia (PCD) caused by the genetic mutation of two main genes of cilia structure, DNAH5 and DNAI1 (Escudier et al., 2009; Rayner et al., 1995; Sharma et al., 2008;). Non-genetic factors defects such as smoking and pathogen infection can also lead to cilia dysfunction, including loss of cells, reduced motility, and shortened length, as observed in COPD and asthma (Chen et al., 2020; Leopold et al., 2009; Milgrim et al., 1995; Simet et al., 2010). Therefore, we first examined the cilia structure to see whether DEPs caused significant structural deformation.

The TEM image of the DEP-exposed cilia showed no prominent structural defects (data not shown). However, as shown in Figs. 2C and 3A, DEP exposure resulted in ciliary dysfunction, such as decreased cells and shortened cilia length. To better address this observation at the molecular level, the expression of cilia structure-related genes, namely

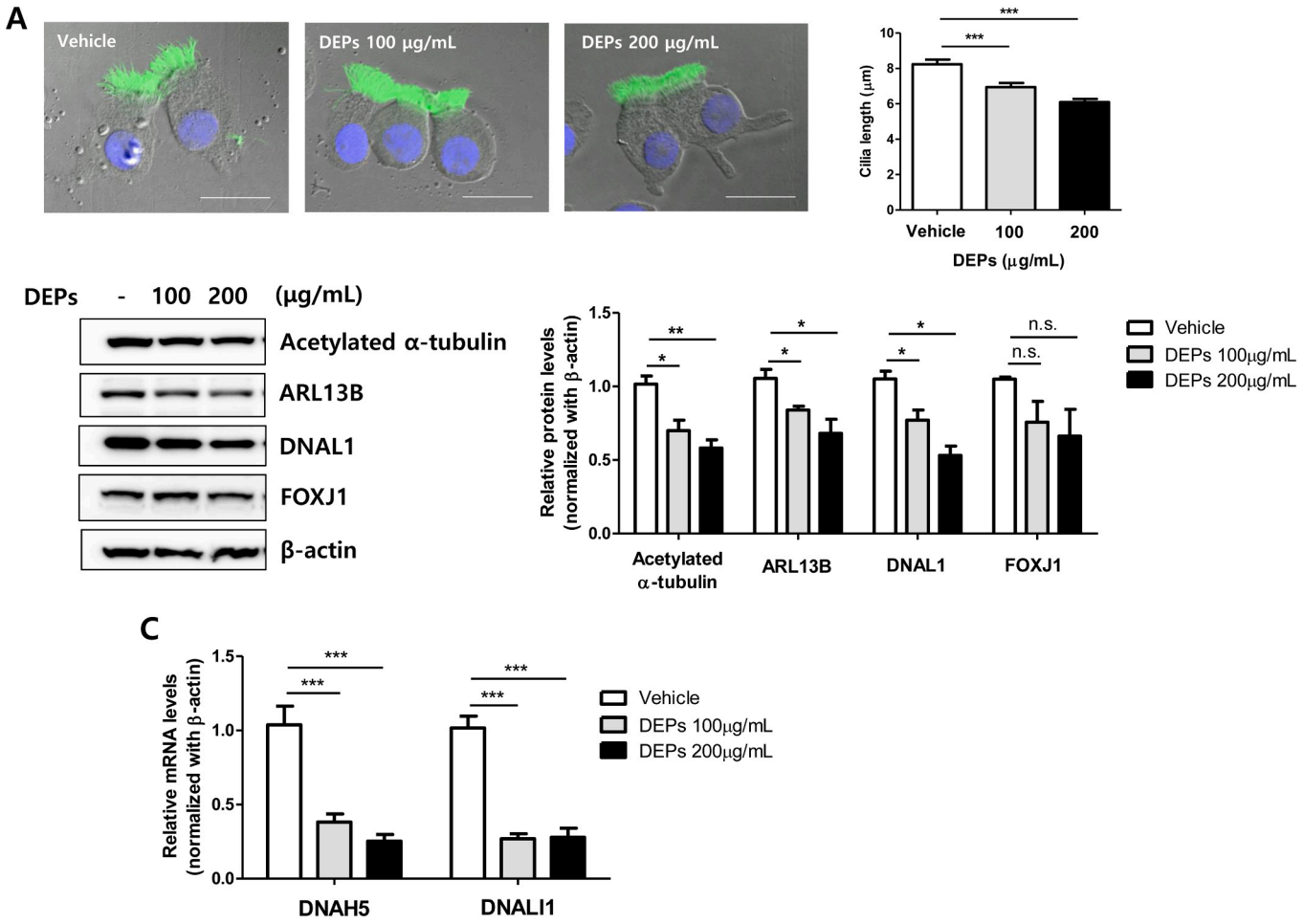

Fig. 3. DEPs inhibit ciliary growth in ALI-cultured NHBEs. (A) DEPs inhibit cilia length. A cytospin centrifuge applied DEP-treated cells on a glass slide and evaluated by immunofluorescence staining. Representative images were merged with acetylated α-tubulin (green), DAPI (blue), and DIC (gray). Bar: 20 μm. Cilia length was measured from 230 cilia in each group (at least 10 cilia per ciliated cell; n=4) using ImageJ software. (B-C) DEPs suppress the expression of cilia-related markers. (B) Western blot analysis of acetylated α-tubulin and ARL13B protein in whole cell lysates after DEP treatment for 72 h (n=4). β-actin was used as a loading control. (C) Quantitative RT-PCR analysis of DNAH5 and DNAL1 mRNA levels in whole cell lysates after DEP treatment for 72 h (n=3). β-actin was used as a loading control. *P < 0.05, **P < 0.01 and ***P < 0.001, compared with vehicle.

acetylated α-tubulin, ARL13B, and FOXJ1, was examined, and their expressions were significantly decreased by DEP, except the FOXJ1, a transcription factor for cilia genes (Fig. 3B). Ciliary membrane protein ARL13B, an ARL family member of small GTPases essential for ciliogenesis, acts as an effector of the elongation of cilia through the extension of the ciliary membrane (Lu et al., 2015). Thus, the repressed expression of ARL13B protein by DEPs in this study may account for the observed shortening of the ciliary length.

Additionally, DEPs significantly inhibited the mRNA expression of DNAH5 and DNALI1, components of the outer dynein arm complex and inner dynein arm complex, respectively (Fig. 3C). It has been reported that the expression of DNALI1 was downregulated in patients with smoking-associated lung diseases (Chen et al., 2018), and epithelial cells exposed to cigarette smoke extracts or poly (I:C) downregulated the expression of cilia structure-related genes, including DNAH5, with shortened cilia length (Brekman et al., 2014; Chen et al., 2020). Thus, the suppression of DNAH5 and DNALI1 expression by DEPs may contribute to the observed shortening of cilia.

However, it also has been reported that knockdown of DNAH5 resulted in immotile cilia in the airway epithelial model (Zahid et al., 2020) and that PM2.5 negatively impacted the ciliary beat function, including ciliary beat frequency and pattern, in nasal epithelium impacting (Jia et al., 2019). Furthermore, the changes in ciliary length have been reported to be associated with ciliary motility (Bottier et al., 2019), and therefore, there still exists a possibility that the DEP-induced shortened cilium and the thickened mucus layer on the multiciliated epithelium lead to a decrease in beating frequency. 2B). In other words, the possibility of DEP-induced hindrance in cilia motility cannot be excluded at this point, and it will be one of the major objectives of our future studies on the biological effect of DEP.

Junctions between adjacent cells physically maintain the airway epithelial barrier and regulate epithelial permeability. These intracellular junctions are comprised of tight junctions, including zona occludins (ZOs), Occludin, Claudins and junction adhesion molecules (JAMs) transmembrane proteins, and adherent junctions, including E-cadherin transmembrane protein (Rezaee and Georas, 2014). Disruption of tight junctions and adherent junctions, such as the decreased expression of ZO-1, ZO-2, Occludin, and E-cadherin in airway epithelium, has been observed in obstructive pulmonary diseases, including asthma and COPD, and is accompanied by impaired mucociliary clearance (Aghapour et al., 2018; Carlier et al., 2021; Rezaee and Georas, 2014).

In the present study, DEPs significantly decreased the expression of epithelial junction proteins ZO-1, Occludin, and E-cadherin (Fig. 4B) and slightly, but significantly, reduced the airway epithelium barrier integrity represented by TEER value at a concentration of 200 μg/mL (Fig. 4C), indicating that DEPs disrupted airway epithelial barrier. Previous studies reported that DEPs disrupt the epithelial barrier in epithelial cells (Lee et al., 2022; Rynning et al., 2018), supporting our

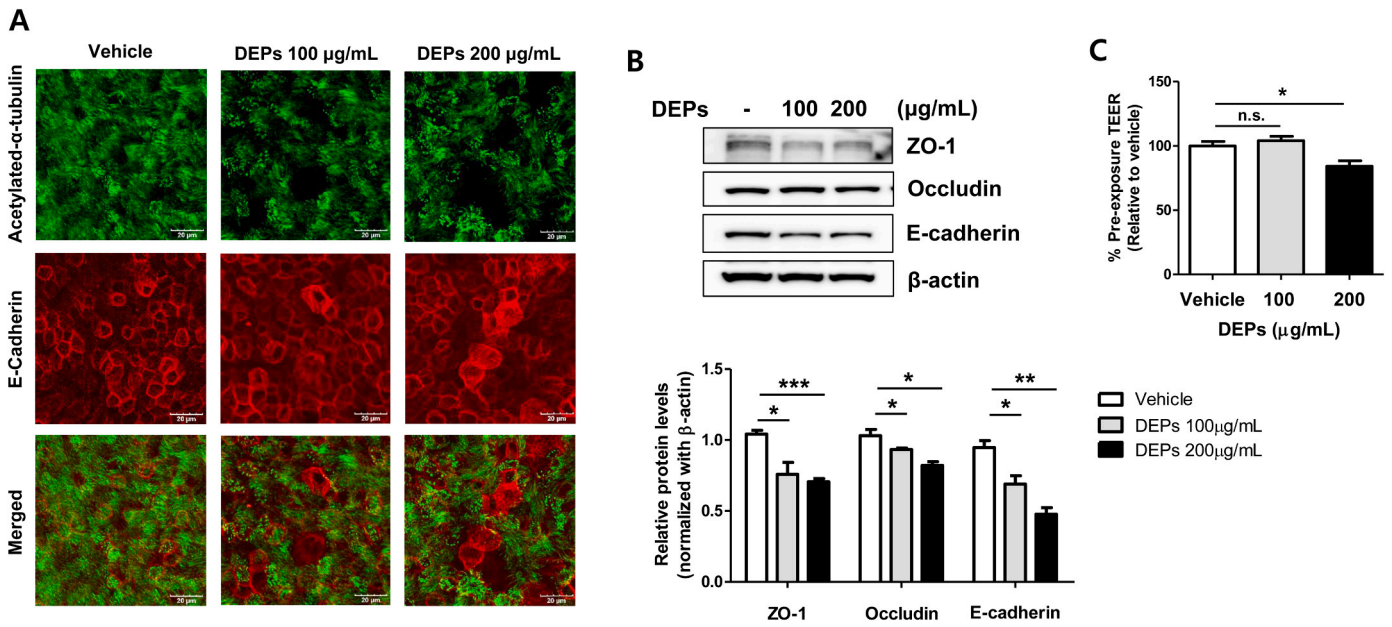

Fig. 4. DEPs reduce the expression of the epithelial junction-related proteins in ALI-cultured NHBEs. (A) Representative immunofluorescence images of acetylated α-tubulin (green) and E-cadherin (red) after DEP treatment for 72 h. Bar: 20 μm. (B) Western blot analysis of ZO-1 and E-cadherin protein in whole cell lysates after DEP treatment for 72 h (n=3). β-actin was used as a loading control. (C) Inhibition of barrier integrity following DEP treatment was determined by TEER measurement (n=4). n.s. > 0.05, *P < 0.05, **P < 0.01 and ***P < 0.001, compared with vehicle.

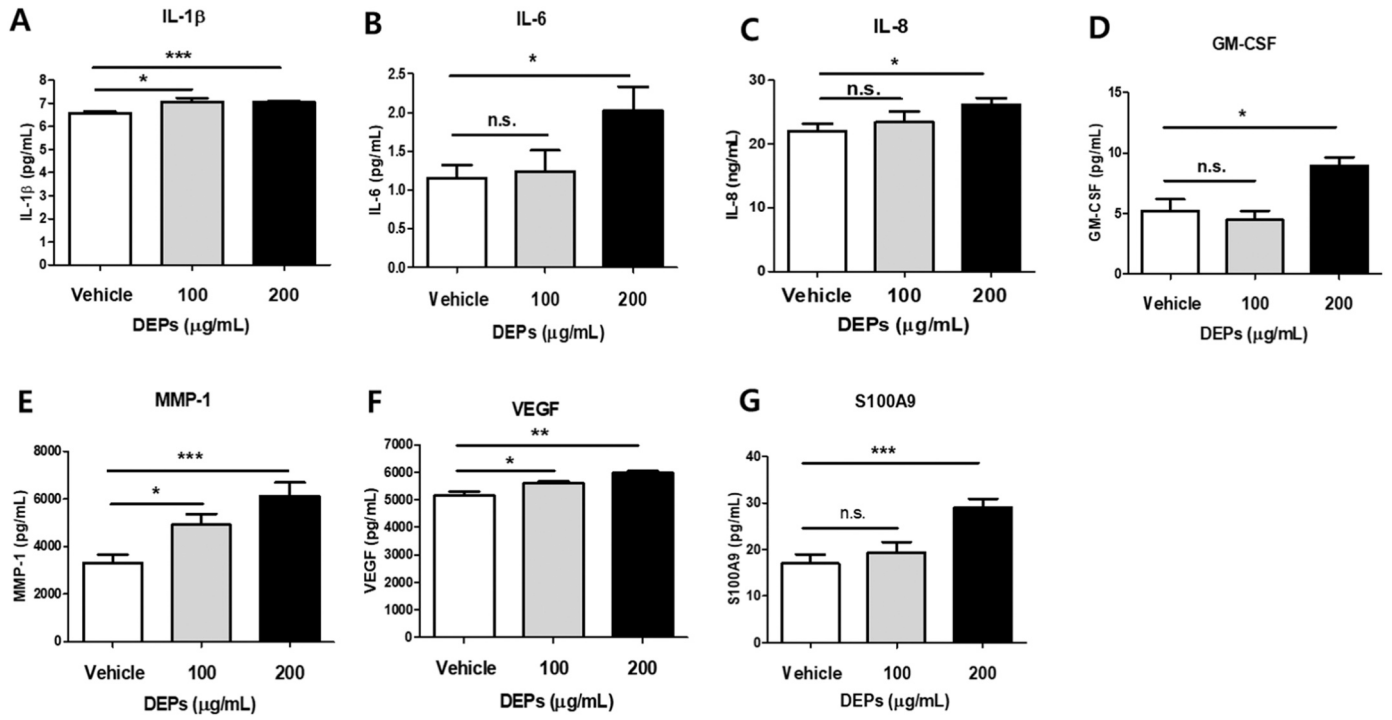

Fig. 5. DEPs increase the release of epithelial-derived inflammatory cytokines and fibrotic mediators. (A-G) Quantitative analysis of cytokines including IL-1β (A), IL-6 (B), IL-8 (C), GM-CSF (D), MMP-1 (E), VEGF (F), and S100A9 (G). Quantitative levels of IL-1β, IL-6, GM-CSF, MMP-1, S100A9, and VEGF were measured in a basolateral medium of ALI-cultured NHBE treated apically with DEPs for 72 h by Luminex assay (n=4). ELISA determined the quantification of IL-8 levels in the basolateral medium (n=4). n.s. > 0.05, *P < 0.05, **P < 0.01 and ***P < 0.001, compared with vehicle.

findings. As to why DEPs only showed a marginal but significant decrease in TEER value at a higher concentration, it is speculated that a relatively short period of treatment (72 h) contributed to such a marginal decrease in TEER value. Considering our experimental protocol was designed to evaluate the detrimental effect of DEPs on the already-established epithelial barrier rather than on the formation of the epithelial barrier, long-term treatment of DEPs may result in more drastic changes in terms of TEER.

Airway epithelium communicates with multiple types of cells, such as immune cells and mesenchymal cells, for the pulmonary defense system. Compromised airway epithelium barrier function stimulates the release of inflammatory and fibrotic mediators, including many

cytokines and chemokines, into the extracellular space (Carlier et al., 2021). The mediators and recruited immune cells promote airway inflammation and act on mesenchymal cells, such as fibroblasts, to stimulate fibrosis, contributing to airway remodeling. In COPD or asthma, the damaged airway epithelium releases pro-inflammatory cytokines (IL-1, IL-8, IL-6, GM-CSF, and TNF-α) and fibrotic factors (TGF-β, PDGF, and MMPs) (Rynning et al., 2018). Furthermore, ambient PM or DEP exposure in airway epithelium upregulates the production of a variety of epithelial cytokines, including IL-1, IL-6, IL-8, IL-25, IL-33, GM-CSF, and TNF-α (De Grove et al., 2018; Leikauf et al., 2020). Among these, IL-1β, IL-6, IL-8, and GM-CSF have been reported to regulate PM-induced signaling, including MAPK, NF-κB, and ROS activation (De Grove et al., 2018). Our data also demonstrate that DEPs significantly increased the production of pro-inflammatory cytokines, namely IL-1β, IL-6, IL-8, and GM-CSF, in the multiciliated epithelium model (Fig. 5A-D). Interestingly, these cytokines released from damaged airway epithelial cells mechanistically trigger profibrotic responses including extracellular matrix (ECM) production, fibroblast proliferation, and collagen synthesis through epithelial-mesenchymal crosstalk (She et al., 2021). In addition to cytokines, DEP exposure enhanced the release of fibrotic factors such as MMP-1, VEGF, and S100A9 (Fig. 5E-G).

Excess activity of MMPs is known to be a pathogenic mediator in destructive pulmonary diseases, and MMP-1 has been reported to be activated by DEPs in bronchial epithelial cells (Amara et al., 2007; Li et al., 2009). In the case of the VEGF, a mediator of angiogenesis and vascular remodeling, its upregulation along with goblet cells hyperplasia, inflammation, and lung fibrosis was observed in mouse models exposed to DEPs, indicating airway inflammation and remolding (Kim et al., 2016). Lastly, S100A9, which activates fibroblast proliferation and collagen formation, is highly upregulated in patients with asthma or idiopathic pulmonary fibrosis (Araki et al., 2021; Xu et al., 2013). These data indicate that DEPs can cause epithelium damage and induce the release of inflammatory cytokines and fibrotic factors to promote immune response and fibrosis. Nevertheless, detailed underlying mechanisms must be further elucidated by studying the communication between airway epithelial cells and immune cells (or fibroblast), possibly with the ALI co-culture model.

This study has a limitation. The experiments with ALI-cultured NHBEs used NHBE cells derived from a single young male. Therefore, further analysis of the effects of DEP exposure by gender or age are required.

5. Conclusion

In the present study, we demonstrated that exposure to DEP impaired mucociliary clearance through ciliary dysfunction, resulting in the secretion of epithelial-derived mediators that can cause airway inflammatory response and fibrosis in a multiciliated epithelium model. The main features of DEP-induced ciliary dysfunction include decreased ciliated cells, shortened ciliary length, and reduced expression of cilia structure-related genes. Our data strongly suggest that DEP can directly damage the airway defense machinery, which may exacerbate lung injury.

Funding

This work was supported by the Research Program funded Korea National Institute of Health (Grant no. 2022-NI-056-00, 2022-NI-056-01).

CRediT authorship contribution statement

Lee Seahyoung: Writing – review & editing. **Son Kuk Hui:** Investigation, Methodology. **Park Eunsook:** Conceptualization, Formal analysis, Investigation, Methodology, Visualization, Writing – original draft. **Kim Bu-Yeo:** Formal analysis, Methodology, Visualization, Writing – original draft. **LIM HYUN JOUNG:** Conceptualization, Funding acquisition, Methodology, Project administration, Supervision, Writing – review & editing. **Uhm Kyung-Ok:** Investigation, Supervision. **Kwak Hyun-Jeong:** Investigation, Supervision. **Lee Joong Won:** Formal analysis, Investigation. **Bang Jihye:** Formal analysis, Investigation. **Hong Se Hyang:** Formal analysis, Investigation.

Declaration of Competing Interest

The authors declare that they have no known competing financial interests or personal relationships that could have appeared to influence the work reported in this paper.

Data Availability

The authors are unable or have chosen not to specify which data has been used.

Acknowledgments

We appreciate Hyun Jung Choi and Jee-woong Kim in the Division of Research Support, Korea National Institute of Health, for assistance with confocal microscopy analysis and TEM, respectively.

Appendix A. Supporting information

Supplementary data associated with this article can be found in the online version at doi:10.1016/j.ecoenv.2024.116090.

References

Adivitiya, Kaushik, M.S., Chakraborty, S., Veleri, S., Kateriya, S., 2021. Mucociliary respiratory epithelium integrity in molecular defense and susceptibility to pulmonary viral infections. Biology 10, 95.
Aghapour, M., Raee, P., Moghaddam, S.J., Hiemstra, P.S., Heijink, I.H., 2018. Airway epithelial barrier dysfunction in chronic obstructive pulmonary disease: role of cigarette smoke exposure. Am. J. Respir. Cell Mol. Biol. 58, 157–169.
Amara, N., Bachoual, R., Desmard, M., Golda, S., Guichard, C., Lanone, S., et al., 2007. Diesel exhaust particles induce matrix metalloprotease-1 in human lung epithelial cells via a NADP(H) oxidase/NOX4 redox-dependent mechanism. Am. J. Physiol. Lung Cell. Mol. Physiol. 293, L170–L181.
Araki, K., Kinoshita, R., Tomonobu, N., Gohara, Y., Tomida, S., Takahashi, Y., et al., 2021. The heterodimer S100A8/A9 is a potent therapeutic target for idiopathic pulmonary fibrosis. J. Mol. Med. 99, 131–145.
Bindea, G., Mlecnik, B., Hackl, H., Charoentong, P., Tosolini, M., Kirilovsky, A., et al., 2009. ClueGO: a cytoscape plug-in to decipher functionally grouped gene ontology and pathway annotation networks. Bioinformatics 25, 1091–1093.
Bottier, M., Thomas, K.A., Dutcher, S.K., Bayly, P.V., 2019. How does cilium length affect beating? Biophys. J. 116, 1292–1304.
Brekman, A., Walters, M.S., Tilley, A.E., Crystal, R.G., 2014. FOXJ1 prevents cilia growth inhibition by cigarette smoke in human airway epithelium in vitro. Am. J. Respir. Cell Mol. Biol. 51, 688–700.
Bustamante-Marin, X.M., Ostrowski, L.E., 2017. Cilia and mucociliary clearance. Cold Spring Harb. Perspect. Biol. 9.
Carlier, F.M., de Fays, C., Pilette, C., 2021. Epithelial barrier dysfunction in chronic respiratory diseases. Front. Physiol. 12, 691227.
Chen, Q., Tan, K.S., Liu, J., Ong, H.H., Zhou, S., Huang, H., et al., 2020. Host Antiviral response suppresses ciliogenesis and motile ciliary functions in the nasal epithelium (Hosts). Front. Cell Dev. Biol. 8, 581340.
Chen, Y., Pan, Y., Ji, Y., Sheng, L., Du, X., 2018. Network analysis of differentially expressed smoking-associated mRNAs, lncRNAs and miRNAs reveals key regulators in smoking-associated lung cancer. Exp. Ther. Med. 16, 4991–5002.
De Grove, K.C., Provoost, S., Brusselle, G.G., Joos, G.F., Maes, T., 2018. Insights in particulate matter-induced allergic airway inflammation: focus on the epithelium. Clin. Exp. Allergy 48, 773–786.
De Hoon, M.J., Imoto, S., Nolan, J., Miyano, S., 2004. Open source clustering software. Bioinformatics 20, 1453–1454.
Escudier, E., Duquesnoy, P., Papon, J.F., Amselem, S., 2009. Ciliary defects and genetics of primary ciliary dyskinesia. Paediatr. Respir. Rev. 10, 51–54.
Ghio, A.J., Dailey, L.A., Soukup, J.M., Stonehuerner, J., Richards, J.H., Devlin, R.B., 2013. Growth of human bronchial epithelial cells at an air-liquid interface alters the response to particle exposure. Part. Fibre Toxicol. 10, 25.
Gray, T.E., Guzman, K., Davis, C.W., Abdullah, L.H., Nettesheim, P., 1996. Mucociliary differentiation of serially passaged normal human tracheobronchial epithelial cells. Am. J. Respir. Cell Mol. Biol. 14, 104–112.
He, R.W., Gerlofs-Nijland, M.E., Boere, J., Fokkens, P., Leseman, D., Janssen, N.A.H., Cassee, F.R., 2020. Comparative toxicity of ultrafine particles around a major airport

in human bronchial epithelial (Calu-3) cell model at the air-liquid interface. Toxicol. Vitr. 68, 104950.
Jia, J., Xia, J., Zhang, R., Bai, Y., Liu, S., Dan, M., et al., 2019. Investigation of the impact of PM2.5 on the ciliary motion of human nasal epithelial cells. Chemosphere 233, 309–318.
Kim, B.G., Lee, P.H., Lee, S.H., Kim, Y.E., Shin, M.Y., Kang, Y., et al., 2016. Long-term effects of diesel exhaust particles on airway inflammation and remodeling in a mouse model. Allergy Asthma Immunol. Res. 8, 246–256.
Kim, B.Y., Lim, H.S., Kim, Y., Kim, Y.J., Koo, I., Jeong, S.J., 2018. Evaluation of animal models by comparison with human late-onset Alzheimer's disease. Mol. Neurobiol. 55, 9234–9250.
Kim, B.Y., Lim, H.S., Kim, Y.J., Sohn, E., Kim, Y.H., Koo, I., Jeong, S.J., 2020. Similarity of therapeutic networks induced by a multi-component herbal remedy, Ukgansan, in neurovascular unit cells. Sci. Rep. 10, 2658.
Kim, J., Choi, H., Choi, D.H., Park, K., Kim, H.J., Park, M., 2021. Application of green tea catechins, polysaccharides, and flavonol prevent fine dust induced bronchial damage by modulating inflammation and airway cilia. Sci. Rep. 11, 2232.
Kim, S.S., Kim, C.H., Kim, J.W., Kung, H.C., Park, T.W., Shin, Y.S., et al., 2017. Airborne particulate matter increases MUC5AC expression by downregulating Claudin-1 expression in human airway cells. BMB Rep. 50, 516–521.
Kim, Y.H., Kim, T., Ji, K.Y., Shin, I.S., Lee, J.Y., Song, K.H., Kim, B.Y., 2022. A time-dependently regulated gene network reveals that Aspergillus protease affects mitochondrial metabolism and airway epithelial cell barrier function via mitochondrial oxidants. Free Radic. Biol. Med 185, 76–89. https://doi.org/10.1016/j.freeradbiomed.2022.04.013. Epub 2022 Apr 27.
Knowles, M.R., Boucher, R.C., 2002. Mucus clearance as a primary innate defense mechanism for mammalian airways. J. Clin. Invest. 109, 571–577.
Lee, M., Lim, S., Kim, Y.S., Khalmuratova, R., Shin, S.H., Kim, I., et al., 2022. DEP-induced ZEB2 promotes nasal polyp formation via epithelial-to-mesenchymal transition. J. Allergy Clin. Immunol. 149, 340–357.
Leikauf, G.D., Kim, S.H., Jang, A.S., 2020. Mechanisms of ultrafine particle-induced respiratory health effects. Exp. Mol. Med. 52, 329–337.
Leopold, P.L., O'Mahony, M.J., Lian, X.J., Tilley, A.E., Harvey, B.G., Crystal, R.G., 2009. Smoking is associated with shortened airway cilia. PLOS ONE 4, e8157.
Li, J., Ghio, A.J., Cho, S.H., Brinckerhoff, C.E., Simon, S.A., Liedtke, W., 2009. Diesel exhaust particles activate the matrix-metalloproteinase-1 gene in human bronchial epithelia in a beta-arrestin-dependent manner via activation of RAS. Environ. Health Perspect. 117, 400–409.
Li, N., Nel, A.E., 2006. The cellular impacts of diesel exhaust particules: beyond inflammation and death. Eur. Respir. J. 27, 667–668.
Loreng, T.D., Smith, E.F., 2017. The central apparatus of cilia and eukaryotic flagella. Cold Spring Harb. Perspect. Biol. 9.
Lu, H., Toh, M.T., Narasimhan, V., Thamilselvam, S.K., Choksi, S.P., Roy, S., 2015. A function for the Joubert syndrome protein Arl13b in ciliary membrane extension and ciliary length regulation. Dev. Biol. 397, 225–236.
Mazzarella, G., Ferraraccio, F., Prati, M.V., Annunziata, S., Bianco, A., Mezzogiorno, A., et al., 2007. Effects of diesel exhaust particles on human lung epithelial cells: an in vitro study. Respir. Med. 101, 1155–1162.
Milgrim, L.M., Rubin, J.S., Small, C.B., 1995. Mucociliary clearance abnormalities in the HIV-infected patient: a precursor to acute sinusitis. Laryngoscope 105, 1202–1208.
Rayner, C.F., Rutman, A., Dewar, A., Cole, P.J., Wilson, R., 1995. Ciliary disorientation in patients with chronic upper respiratory tract inflammation. Am. J. Respir. Crit. Care Med. 151, 800–804.
Rayner, R.E., Makena, P., Prasad, G.L., Cormet-Boyaka, E., 2019. Optimization of normal human bronchial epithelial (NHBE) cell 3D cultures for in vitro lung model studies. Sci. Rep. 9, 500.
Rezaee, F., Georas, S.N., 2014. Breaking barriers. New insights into airway epithelial barrier function in health and disease. Am. J. Respir. Cell Mol. Biol. 50, 857–869.
Rynning, I., Neca, J., Vrbova, K., Libalova, H., Rossner, P., Jr, Holme, J.A., et al., 2018. In vitro transformation of human bronchial epithelial cells by diesel exhaust particles: gene expression profiling and early toxic responses. Toxicol. Sci. 166, 51–64.
Schamberger, A.C., Staab-Weijnitz, C.A., Mise-Racek, N., Eickelberg, O., 2015. Cigarette smoke alters primary human bronchial epithelial cell differentiation at the air-liquid interface. Sci. Rep. 5, 8163.
Sharma, N., Berbari, N.F., Yoder, B.K., 2008. Ciliary dysfunction in developmental abnormalities and diseases. Curr. Top. Dev. Biol. 85, 371–427.
She, Y.X., Yu, Q.Y., Tang, X.X., 2021. Role of interleukins in the pathogenesis of pulmonary fibrosis. Cell Death Discov. 7, 52.
Simet, S.M., Sisson, J.H., Pavlik, J.A., Devasure, J.M., Boyer, C., Liu, X., et al., 2010. Long-term cigarette smoke exposure in a mouse model of ciliated epithelial cell function. Am. J. Respir. Cell Mol. Biol. 43, 635–640.
Steiner, S., Bisig, C., Petri-Fink, A., Rothen-Rutishauser, B., 2016. Diesel exhaust: current knowledge of adverse effects and underlying cellular mechanisms. Arch. Toxicol. 90, 1541–1553.
Stewart, C.E., Torr, E.E., Mohd Jamili, N.H., Bosquillon, C., Sayers, I., 2012. Evaluation of differentiated human bronchial epithelial cell culture systems for asthma research. J. Allergy (Cairo 2012, 943982.
Wu, T., Hu, E., Xu, S., Chen, M., Guo, P., Dai, Z., et al., 2021. clusterProfiler 4.0: A universal enrichment tool for interpreting omics data. " Innov 2, 100141. https://doi.org/10.1016/j.xinn.2021.100141.
Xu, X., Chen, H., Zhu, X., Ma, Y., Liu, Q., Xue, Y., et al., 2013. S100A9 promotes human lung fibroblast cells activation through receptor for advanced glycation end-product-mediated extracellular-regulated kinase ½, mitogen-activated protein-kinase and nuclear factor-κB-dependent pathways. Clin. Exp. Immunol. 173, 523–535.
Yang, L., Li, C., Tang, X., 2020. The impact of PM2.5 on the host defense of respiratory system. Front. Cell Dev. Bio. 8, 91.
Zahid, M., Feinstein, T.N., Oro, A., Schwartz, M., Lee, A.D., Lo, C.W., 2020. Rapid ex-vivo ciliogenesis and dose-dependent effect of Notch inhibition on ciliogenesis of respiratory epithelia. Biomolecules 10.
Zarcone, M.C., Duistermaat, E., van Schadewijk, A., Jedynska, A., Hiemstra, P.S., Kooter, I.M., 2016. Cellular response of mucociliary differentiated primary bronchial epithelial cells to diesel exhaust. Am. J. Physiol. Lung Cell. Mol. Physiol. 311, L111–L123.